ChemPubSoc Europe

DOI: 10.1002/chem.201704381

CHEMISTRY
A European Journal
Communication

Redox-Flow Batteries

An Fe^{III} Azamacrocyclic Complex as a pH-Tunable Catholyte and Anolyte for Redox-Flow Battery Applications

Pavel B. Tsitovich, Anjula M. Kosswattaarachchi, Matthew R. Crawley, Timothy Y. Tittiris, Timothy R. Cook,* and Janet R. Morrow*[a]

Abstract: A reversible Fe^{3+}/Fe^{2+} redox couple of an azamacrocyclic complex is evaluated as an electrolyte with a pH-tunable potential range for aqueous redox-flow batteries (RFBs). The Fe^{III} complex is formed by 1,4,7-triazacyclononane (TACN) appended with three 2-methyl-imidazole donors, denoted as Fe(Tim). This complex exhibits pH-sensitive redox couples that span $E_{1/2}(Fe^{3+}/Fe^{2+}) = 317$ to -270 mV vs. NHE at pH 3.3 and pH 12.8, respectively. The 590 mV shift in potential and kinetic inertness are driven by ionization of the imidazoles at various pH values. The Fe^{3+}/Fe^{2+} redox is proton-coupled at alkaline conditions, and bulk electrolysis is non-destructive. The electrolyte demonstrates high charge/discharge capacities at both acidic and alkaline conditions throughout 100 cycles. Given its tunable redox, fast electrochemical kinetics, exceptional stability/cyclability, this complex is promising for the design of aqueous RFB catholytes and anolytes that utilize the earth-abundant element iron.

Azamacrocyclic ligands provide a robust scaffold for coordination of first-row transition-metal ions.[1] While a great deal of attention has been directed towards the development of first-row transition-metal macrocyclic complexes as MRI contrast agents[2] and redox-active supramolecular devices,[3] this class of water-soluble and extremely stable coordination compounds has found limited application in energy research. This absence is surprising given the rich coordination and redox chemistry accessible for the Fe^{3+}/Fe^{2+} and Co^{3+}/Co^{2+} azamacrocyclic complexes.[4] Moreover, a wide range of redox potentials makes these remarkably stable complexes suitable for various electron-transfer (ET) and energy-related applications. The low cost and availability of first-row transition-metal ions makes them attractive in energy applications when compared to less abundant heavy elements.

[a] Dr. P. B. Tsitovich, A. M. Kosswattaarachchi, M. R. Crawley, T. Y. Tittiris, Prof. Dr. T. R. Cook, Prof. Dr. J. R. Morrow
Department of Chemistry
University at Buffalo, the State University of New York
Buffalo, NY 14260 (USA)
E-mail: trcook@buffalo.edu
jmorrow@buffalo.edu

Supporting information and the ORCID number(s) for the author(s) of this article can be found under: https://doi.org/10.1002/chem.201704381.

A redox flow battery (RFB) is an electrochemical energy storage device that is based on the oxidation and reduction of redox-active molecules.[5] In a RFB, electrolyte solutions containing active components are pumped across electrodes to charge or discharge the device.[6] The main advantage of flow batteries is the ability to scale power and energy densities orthogonally. Redox couples based on first-row transition-metal ions, such as V^{3+}/V^{2+}, V^{5+}/V^{4+}, Cr^{3+}/Cr^{2+}, Mn^{3+}/Mn^{2+}, Fe^{3+}/Fe^{2+}, and Cu^{2+}/Cu^{+}, have been utilized as electrolytes in RFB technology.[5] Although it is possible to use redox species of two different metallic elements, cross-contamination of the electrolytes through the ion-exchange membrane results in irreversible Coulombic efficiency losses that ultimately require a recharging of electrolyte solution. This problem can be overcome by use of a single metal for both catholytes and anolytes, resulting in all-vanadium, all-chromium, all-lead, and all-copper RFBs.[5b,c] Iron-based redox couples can also be used as either anolytes or catholytes depending on their redox potentials.[5c,7] All-iron RFBs involving Fe^{2+}/Fe^{0} and Fe^{3+}/Fe^{2+} couples have been designed.[8] Along with the problems associated with the deposition and dissolution of metallic iron, the hydrogen evolution reaction (HER) becomes competitive under the reducing conditions required for Fe^{2+}/Fe^{0} cycling. Recently, all-iron RFB electrolytes based on Fe^{3+}/Fe^{2+} couples produced by two different types of ligands have been reported.[7b] Herein, the strategy of employing Fe coordination chemistry motivates the synthesis and study of a TACN-based complex (Scheme 1). This complex is unusual in that it is stable across a wide range of pH values and the pendant groups on the ligands provide sites for proton-coupled ET that result in tunable Fe^{3+}/Fe^{2+} redox potentials that shift by 590 mV from pH 3.3 to 12.8. The magnitude of this shift enables this complex to serve as a catholyte under acidic conditions and more importantly, as a rare example of a water-soluble alkaline-stable negolyte under basic conditions. This is an outstanding challenge in the aqueous RFB community, since very few organic[9] and iron-based inorganic[5c,7b] compounds with such properties have been reported.

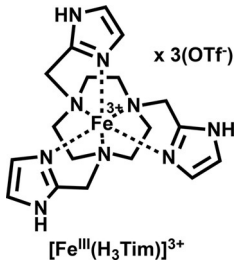

$[Fe^{III}(H_3Tim)]^{3+}$

Scheme 1. $[Fe(H_3Tim)](OTf)_3$.

Azamacrocyclic ligands form transition-metal complexes with enhanced thermodynamic and kinetic stability owing to

chelation, especially when pendant Lewis-basic sites are present.[10] In such cases, the metal ion is buried within the ligand scaffold, attenuating dissociation and ultimately manifesting in stable redox cycling. The ligand design used herein is based on TACN (1,4,7-triazacyclononane) appended with three 1*H*-pyrazol-3-methylene donors, motivated by the observation that similar macrocycles result in stable Co^{III} and Fe^{III} complexes under aerobic conditions.[11] The ligand, abbreviated as H_3Tim in its neutral form, readily reacts with either Fe^{II} or Fe^{III} salts (Supporting Information, Scheme S1), producing the $[Fe^{III}(H_3Tim)]^{3+}$ complex under aerobic conditions. This complex has a magnetic moment of $\mu_{eff} = 2.9 \pm 0.1$ BM at 25 °C, measured using Evan's method in solution,[12] which is characteristic of low-spin Fe^{III}. The crystal structure corresponds to $[Fe^{III}(H_3Tim)]^{3+}$ with all three imidazole rings protonated (Figure 1), as suggested by both residual electron density and

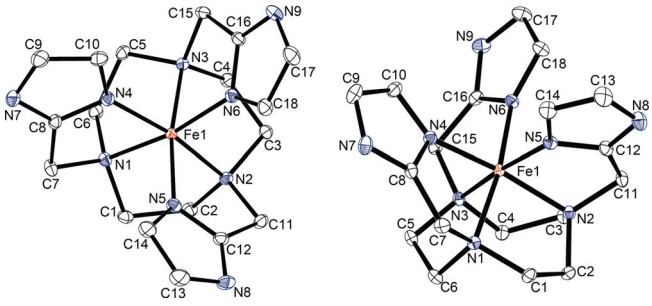

Figure 1. ORTEP of $[Fe(H_3Tim)](OTf)_3$.[21] Ellipsoids are set at 50% probability; hydrogen atoms and counterions are omitted for clarity.

the three triflate counterions present in the unit cell. The complex crystallized in the triclinic centrosymmetric $P\bar{1}$ space group (Supporting Information, Table S1). The central Fe^{III} ion exhibited a distorted octahedral coordination environment based on both bond lengths and angles (Supporting Information, Tables S2, S3), as well as by the twist angle (θ) of 49.3° on average that deviates from an ideal octahedron, which is characterized by $\theta = 60°$ (Supporting Information, Figure S11).

The UV/Vis absorbance spectra and cyclic voltammograms (CVs) of the Fe(Tim) complexes are sensitive to pH, wherein Fe(Tim) represents all of the $[Fe^x(H_nTim)]^{m+}$ species discussed. The electronic absorbance spectra change markedly with pH, demonstrating clear isosbestic points that attest to an equilibrium between two species of different protonation states that exists from pH 2.7 to pH 7.6 (Figure 2). Based on these spectral changes at $\lambda = 380$ nm, a pK_a of 6.7 ± 0.1 for the $[Fe^{III}(H_3Tim)]^{3+}$ to $[Fe^{III}(H_2Tim)]^{2+}$ ionization was obtained from the non-linear regression analysis of the spectral titration curve (Figure 2B). This change is assigned to the deprotonation of one of the three imidazole pendants. As the pH is raised further, a more complex behavior emerges (Supporting Information, Figure S1). The bands become blue-shifted at pH > 7.6, attributed to two successive proton-transfer equilibria (Supporting Information, Figure S2), assigned to further deprotonation of two imidazole rings. These ionizations at alkaline conditions are studied further by using pH-potentiometric titration as dis-

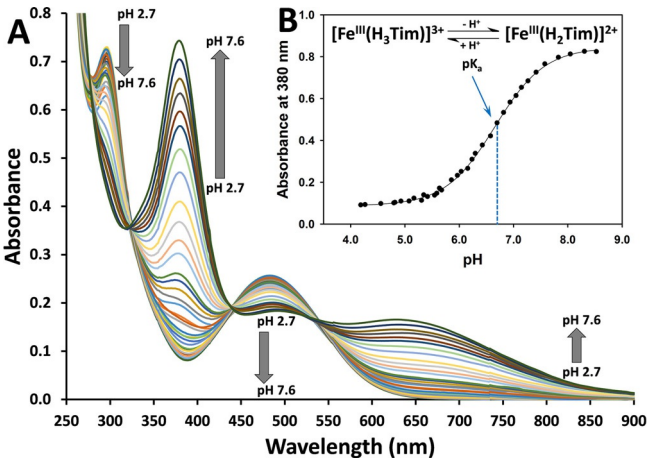

Figure 2. A) The pH dependence of 0.34 mM Fe(Tim) UV/Vis spectrum at pH 2.7–7.6. Conditions: 20 mM MES, 100 mM NaCl in H_2O at 37 °C. B) pH dependence of the absorbance intensity at $\lambda = 380$ nm with a fit of the data to a single ionization model (Supporting Information, Eq. S2) that gives a pK_a of 6.7 ± 0.1.

cussed below. Moreover, the UV/Vis studies are used to elucidate the stability of the complex at different pH values. Notably, no significant changes in the absorption spectra were observed for pH 3.0 or pH 12.5 solutions over the course of 24 hours. When the pH is adjusted from 12.5 back to pH 3.0, the UV/Vis spectrum of the complex matches the original spectrum at pH 3.0, evidence that the fully deprotonated Fe^{III} complex is stable even at highly alkaline conditions (Supporting Information, Figure S3). Such stable ferric complexes with six nitrogen donors are rare. At basic pH, the deprotonation of the imidazole donor groups produces an anionic azamacrocyclic ligand that has high binding affinity to the strongly Lewis acidic Fe^{III} ion. Although subsequent studies focused on pH values between 3.0 and 12.8, the $[Fe^{III}(H_3Tim)]^{3+}$ complex also stays intact even at pH ≤ 3. The Fe(Tim) complex demonstrates pH-dependent solubility in water of 0.27 M and 0.11 M at pH 3.3 and pH 12.0, respectively.

To further study the ionizations, pH-potentiometric titration of the Fe^{III} complex was carried out in aqueous solution. Three ionization events occur in the range of pH 3.0 to 12.0 (Supporting Information, Figure S4). This clearly indicates that $[Fe^{III}(H_3Tim)]^{3+}$ acts as a tribasic acid in solution with pK_a values of 6.8 ± 0.1, 8.4 ± 0.2, and 9.8 ± 0.2 of three imidazole imine groups (Scheme 2) as obtained from the data fitting (Supporting Information, Figure S4). The value of $pK_{a1} = 6.8 \pm 0.1$ is in agreement with that obtained from the UV/Vis pH-titration data analysis (Figure 2). From the speciation diagram in the Supporting Information, Figure S4B, this complex exists primarily in its protonated form $[Fe^{III}(H_3Tim)]^{3+}$ at pH < 4.0 and fully deprotonated form $[Fe^{III}(Tim)]$ at pH > 11.5, while all four species, including $[Fe^{III}(H_2Tim)]^{2+}$ and $[Fe^{III}(HTim)]^{+}$, are present in different ratios at the intermediate pH values (Scheme 2). At pH > 11.0, the Fe^{III} complex shows an additional ionization, which is assigned to the formation of a hydroxide adduct, formulated as the $[Fe^{III}(Tim)(OH)]^{-}$ species. The hydroxide ion in this species is likely bound to the macrocyclic complex

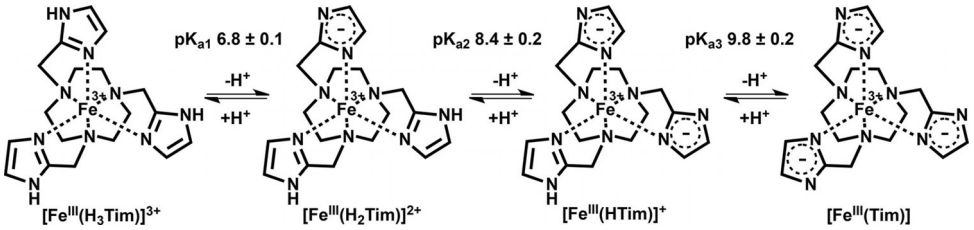

Scheme 2. Speciation of Fe(Tim) in water.

through outer-sphere hydrogen bonding interactions, similar to that observed for an outer-sphere water in analogous complexes.[11b]

Given the exceptional stability of this Fe^{3+} complex over a large pH range, the electrochemical properties were studied in aqueous solution. At acidic conditions of pH 3.3, the CVs demonstrate a single wave with $E_{1/2}(Fe^{3+}/Fe^{2+}) = 317 \pm 5$ mV vs. NHE (Figure 3) corresponding to a fully-protonated $[Fe^{III}(H_3Tim)]^{3+}$ state. This is a fully reversible Fe^{3+}/Fe^{2+} redox reaction based on the insignificant shift in peak potential at different scan rates (Supporting Information, Figure S5). At pH 6.5 < pK_{a1}, the complex is present in a predominantly protonated $[Fe^{III}(H_3Tim)]^{3+}$ form with some $[Fe^{III}(H_2Tim)]^{2+}$ species present (Supporting Information, Figure S4B). The redox potential of $E_{1/2}(Fe^{3+}/Fe^{2+}) = 315 \pm 6$ mV vs. NHE, pH 6.5, is constant at different scan rates, which is characteristic of a fully reversible ET reaction based on peak separation (Supporting Information, Figure S7). A single wave is also observed at strongly alkaline pH values (Figure 3). However, the Fe^{3+}/Fe^{2+} redox reaction becomes quasi-reversible at pH ≥ 12.0, since the variation of the scan rate affects the peak separation (Supporting Information, Figures S8, S9). At pH values higher than pK_{a3}, the complex is in predominantly fully-deprotonated $[Fe^{III}(Tim)]$ form (Supporting Information, Figure S4B) which has $E_{1/2}(Fe^{3+}/Fe^{2+}) = -270 \pm 5$ mV vs. NHE at pH 12.8, 25 °C. Notably, the $E_{1/2}(Fe^{3+}/Fe^{2+})$ values of $[Fe^{III}(H_3Tim)]^{3+}$ demonstrate nearly no change at 3.3 ≤ pH ≤ 7.2. However, the second CV wave assigned to the $[Fe^{III}(H_2Tim)]^{2+}$ species appears at pH values higher than pK_{a1} (Figure 3). Thus, the voltammograms at 7.2 ≤ pH ≤ 10.8 show multiple pH-dependent half-waves. Moreover, the variation of scan rates has no effect on the shapes of the CV waves of multiple Fe(Tim) species as shown at pH 9.8 (Supporting Information, Figure S10). The observation of multiple waves is attributed to the presence of several Fe^{3+}/Fe^{2+} redox couples produced by $[Fe^{III}(H_2Tim)]^{2+}$, $[Fe^{III}(HTim)]^{+}$, and $[Fe^{III}(Tim)]$ species that exist at equilibrium in aqueous solution prior to the ET event, as in the Supporting Information, Figure S4. Our observations differ from a single CV wave of a benzimidazole-coordinated Ru^{3+}/Ru^{2+} couple, which demonstrated a simple pH-gradient shift of redox potential.[13] However, the voltammograms of Fe(Tim) are similar to multiple CV waves observed for Fe^{3+}/Fe^{2+} couples furnished by imidazole-based tripodal ligands.[14] The multiple CV waves likely result from two factors: an equilibrium of Fe^{III} species of different protonation states, and slow proton-transfer reactions.

The Nernst equation predicts a −59 mV/pH unit shift for a single proton-coupled ET event. Within the 7.2 ≤ pH ≤ 10.8 pH region, the potentials of three Fe^{3+}/Fe^{2+} couples change linearly with the slopes of about −40 mV/pH unit, which is an indication of a slow proton-transfer process (Figure 3B). Only a single wave is present at pH ≥ 10.8 > pK_{a3}, suggesting that one species, $[Fe^{III}(Tim)]$, predominates in solution at alkaline condi-

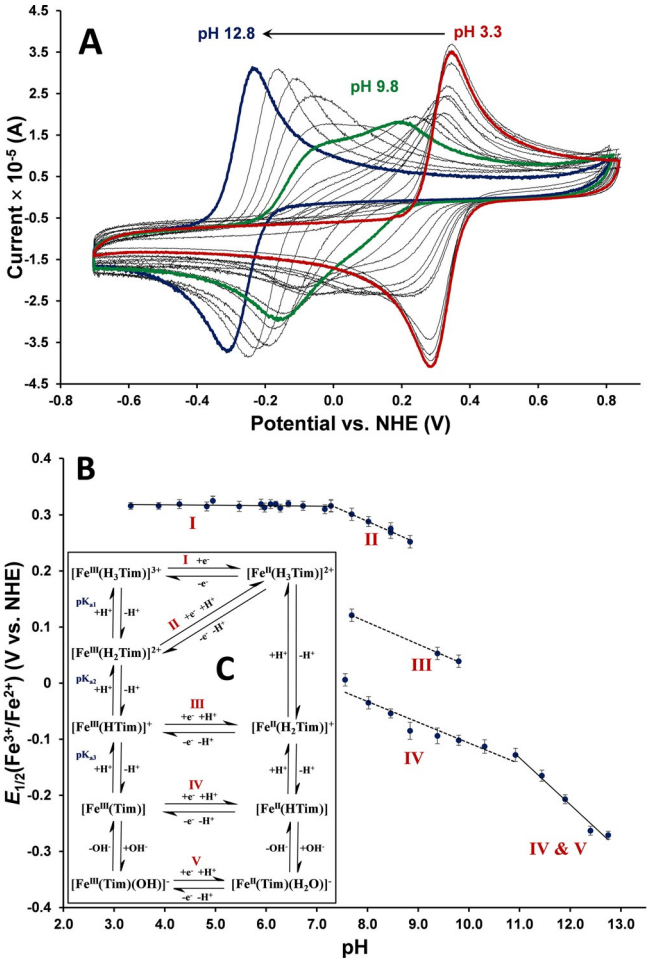

Figure 3. A) Cyclic voltammograms of 2.5 mM Fe(Tim) as a function of pH in 1.0 M KCl aqueous solution at 25 °C, 100 mV s^{-1} scan rate; $E_{1/2}(Fe^{3+}/Fe^{2+}) = 317 \pm 5$ mV vs. NHE at pH 3.3 and $E_{1/2}(Fe^{3+}/Fe^{2+}) = -270 \pm 5$ mV vs. NHE at pH 12.8. B) Fe^{3+}/Fe^{2+} reduction potentials of Fe(Tim) as a function of pH. The lines represent linear fits of the data for different proton-coupled ET reactions. C) Proposed redox and proton-transfer reactions of Fe(Tim). Roman numerals represent reactions in different segments of Pourbaix diagram (B).

tions. At pH $\geq$10.8, the redox potentials of the Fe^{3+}/Fe^{2+} couple decrease linearly with a slope close to −84 mV/pH unit, indicating a one-electron process coupled with the transfer of at least one proton, which is based on the Nernstian prediction.[15] The proton coupling is assigned to a significant increase in the imidazole pK_a upon reduction to Fe^{II} as shown previously.[14] Given that the population of $[Fe^{III}(Tim)(OH)]^-$ species increases at strongly alkaline pH, the proton transfer might represent a more complicated speciation with the formation of $[Fe^{II}(Tim)(H_2O)]^-$.[11b] Fitting of the multiple CV waves, together with the speciation obtained from pH-potentiometric titrations (Supporting Information, Figure S4B) allowed assignment of redox- and proton-coupled reactions at the studied pH range as shown in Figure 3C. Overall, the CV studies show that the Fe^{3+}/Fe^{2+} redox system is electrochemically stable over a wide pH range, while reversible and quasi-reversible electrochemical properties are observed when the complex is completely protonated (pH $\leq$6.5) and deprotonated (pH $\geq$11.5), respectively.

Bulk cycling of Fe(Tim) aqueous solutions was performed at both acidic and basic pH values wherein the fully protonated and fully deprotonated species are present, respectively, at these conditions. These experiments monitor the overall long-term electrochemical stability of the oxidized/reduced species, which is a critical determinant of efficiency of a RFB electrolyte.[16] Cycling was performed up to a 50% state of charge by applying alternate potentials of −0.2 V and 0.5 V vs. NHE at pH 4.0, and −0.5 V and 0.2 V vs. NHE at pH 12.0 to reduce and oxidize, respectively. Figure 4A (top) shows the charge vs. time curves obtained for 100 cycles at pH 4.0. After the first few cycles, Coulombic efficiencies approached 100%. The near-unity efficiency indicates that the stability of the Fe^{II} species extends beyond the CV timescale and is maintained over the course of 7 hours. Moreover, CV profiles collected before and after bulk cycling do not change, further confirming the high stability of the electrolyte. Similarly, bulk cycling and cyclic voltammetry was carried out on the electrolyte solution at pH 12.0 (Figure 4, bottom). Charge vs. time curves were stable for all 100 cycles, and Coulombic efficiency was nearly 100% in all cycles over the course of 12 hours, demonstrating that the redox process is reversible in the completely deprotonated state as well. CVs obtained before and after cycling are unperturbed, suggesting electrochemical reversibility and stability of Fe(Tim) at pH 12.0. The diffusion coefficients were found to be 3.8×10^{-6} and 4.9×10^{-5} $cm^2\cdot s^{-1}$ at pH 4.0 and pH 12.0, respectively (Supporting Information, Figures S6, S8).

Accordingly, the heterogeneous ET rate constants of 4.3×10^{-2} and 3.0×10^{-2} $cm\,s^{-1}$ were found at these acidic and alkaline pH conditions. The fast electrochemical kinetics evidenced by the large ET rate constants and diffusion coefficients of both $[Fe^{III}(H_3Tim)]^{3+}$ and $[Fe^{III}(Tim)]$ match the properties of some recently developed inorganic electrolytes,[7b,17] which is promising for the reduction of polarization overpotential caused by the charge transfer and mass transport resistances.

This work pioneers the development of stable aza-macrocyclic complexes for RFBs. The Fe(Tim) complex is unique in its ability to act as either a catholyte, or an anolyte, depending on the working pH of the cell. Recent developments of aqueous pH-dependent redox systems based on organic compounds, such as viologen derivatives,[9a,18] anthraquinone derivatives[19] and flavin mononucleotide,[9c] among others,[6] resulted in RFB electrolytes with anodic potentials. Alkaline-stable iron-based electrolytes are rare among aqueous RFBs, with only a few compounds reported to date.[5b,c] Although Fe-based negolytes are attractive owing to the low cost associated with earth-abundant first-row metals, if acidic conditions are used, the hydrogen evolution reaction competes with the Fe^{3+}/Fe^{2+} couple, resulting in problematic H_2 formation. The HER potential can be shifted by using basic conditions, however, Fe-based negolytes are plagued by precipitation under alkaline conditions. Therefore, there is a critical need to identify alkaline-stabile Fe-based negolytes which alleviate HER concerns yet maintain high solubility and stability for long-term cycling. Prior to this work, the two most negative Fe^{3+}/Fe^{2+} couples

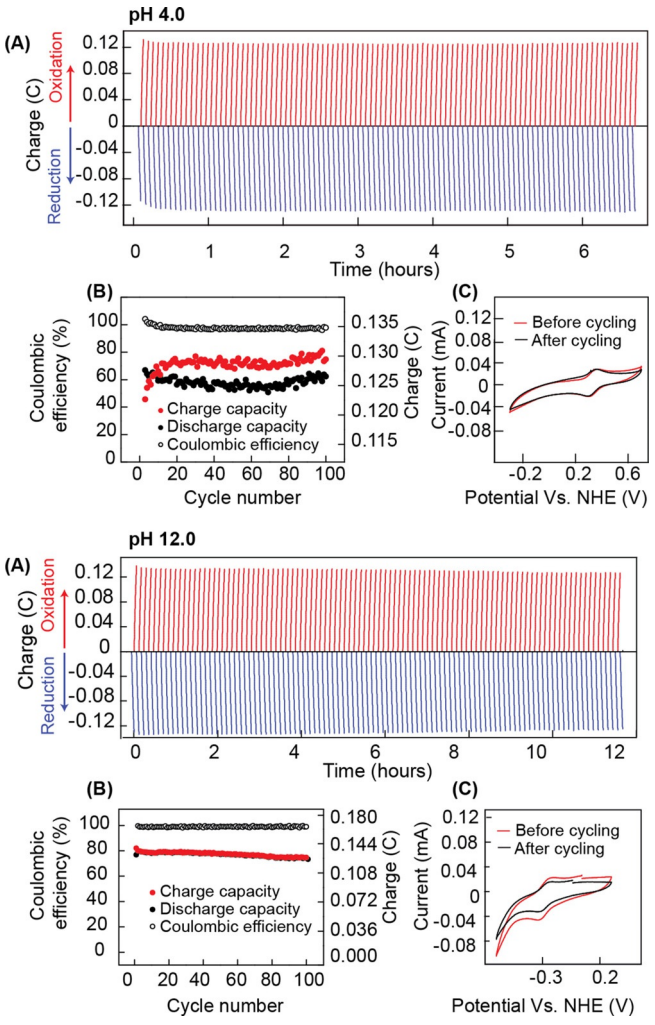

Figure 4. A) Bulk reduction and oxidation cycling between the Fe^{3+} and Fe^{2+} states at pH 4.0 (top) and pH 12.0 (bottom) of 1.0 mM Fe(Tim). Red and blue lines represent about 50% state of charge in each of 100 cycles of bulk oxidized/reduced states. Conditions: 1.0 M KCl in distilled water in the working electrode compartment. B) Cyclic voltammograms obtained before/after bulk cycling: scan rate = 300 $mV\,s^{-1}$. C) Capacity retention and Coulombic efficiency for 100 cycles at pH 4.0 and pH 12.0.

under alkaline conditions were $[Fe^{III}(EDTA)]^{-}/[Fe^{II}(EDTA)]^{2-}$ at 0.14 V vs. NHE,[5c] and recently developed Fe^{3+}/Fe^{2+} redox couple of Fe(TEOA) stabilized by triethanolamine at −0.86 vs. NHE, which is well within the range of H_2 evolution.[7b] This work places the Fe^{3+}/Fe^{2+} couple within the negative potential range for high open circuit potentials, yet not so reducing that HER is active when graphite electrodes are used. The $E_{1/2}(Fe^{3+}/Fe^{2+})$ of −270 mV is close to the optimal inorganic V^{3+}/V^{2+} and Cr^{3+}/Cr^{2+} redox couples that were previously utilized as anolytes.[5b,c] While some anthraquinone derivatives have potentials as low as −0.70 V vs. NHE under alkaline conditions,[19] less negative potentials are required to minimize HER. Notably, methyl viologen with a redox potential of −0.45 V vs. NHE at neutral pH is a gold standard among organic anolytes for aqueous RFBs.[18a] Further tuning of redox potentials of Fe(Tim) is feasible, since the peripheral substitution of the pendant groups, or macrocycle itself is chemically accessible. Furthermore, given the direct relationship between energy density and concentration, a relatively good water solubility (ca. 0.1–0.3 M) of the different ionization forms of Fe(Tim) is improvable via chemical modifications of the ligand.

While it is desirable for the molecular weight of the active species to be low for the increased capacity of the battery, Fe(Tim) is 2.3-fold heavier than methyl viologen[9a] and 6% lighter than flavin mononucleotide.[9c] This places it well within the weight range of commonly used electrolyes. As an added benefit, as the size of the active species is increased, membrane crossover will be attenuated from a size-exclusion standpoint, resulting in a positive impact on overall efficiency of Fe(Tim). Given the 590 mV shift in potential of species at alkaline and acidic conditions, a symmetric RFB device operating at different pH conditions is feasible. This is due to the recent progress in the design of anion exchange membranes, which are capable of maintaining different pH values for the posolyte and negolyte sides of a RFB.[7a,20] Notably, the current system is not limited to a symmetric device, but rather may serve as either the catholyte or anolyte with a second active species operating at the same pH, in which case traditional membranes are also viable.

Acknowledgements

J.R.M. thanks the NSF (CHE-1310374 and CHE 1710224) for support of this work. T.R.C. thanks the University at Buffalo and State University of New York (SUNY) Research Foundation for support. The authors thank SUNY Fredonia for the use of their X-ray diffractometer.

Conflict of interest

The authors declare no conflict of interest.

Keywords: azamacrocycles · iron complexes · pH-tunable potential · proton-coupled electron transfer · redox-flow batteries

[1] S. J. Archibald, Annual Reports Section "A" (*Inorganic Chemistry*) **2008**, *104*, 272 – 296.
[2] a) P. B. Tsitovich, J. R. Morrow, *Inorg. Chim. Acta* **2012**, *393*, 3 – 11; b) S. J. Dorazio, A. O. Olatunde, P. B. Tsitovich, J. R. Morrow, *JBIC J. Biol. Inorg. Chem.* **2014**, *19*, 191 – 205; c) J. R. Morrow, P. B. Tsitovich, in Chemical Exchange Saturation Transfer Imaging: Advances and Applications, Pan Stanford Publishing, **2017**, pp. 257 – 282.
[3] B. Korybut-Daszkiewicz, R. Bilewicz, K. Woźniak, *Coord. Chem. Rev.* **2010**, *254*, 1637 – 1660.
[4] a) G. A. Lawrance, P. A. Lay, A. M. Sargeson, *Inorg. Chem.* **1990**, *29*, 4808 – 4816; b) P. V. Bernhardt, K.-I. Chen, P. C. Sharpe, *JBIC J. Biol. Inorg. Chem.* **2006**, *11*, 930; c) P. B. Tsitovich, P. J. Burns, A. M. McKay, J. R. Morrow, *J. Inorg. Biochem.* **2014**, *133*, 143 – 154.
[5] a) P. Leung, X. Li, C. Ponce de Leon, L. Berlouis, C. T. J. Low, F. C. Walsh, *RSC Adv.* **2012**, *2*, 10125 – 10156; b) W. Wang, Q. Luo, B. Li, X. Wei, L. Li, Z. Yang, *Adv. Funct. Mater.* **2013**, *23*, 970 – 986; c) G. L. Soloveichik, *Chem. Rev.* **2015**, *115*, 11533 – 11558.
[6] J. Winsberg, T. Hagemann, T. Janoschka, M. D. Hager, U. S. Schubert, *Angew. Chem. Int. Ed.* **2017**, *56*, 686 – 711; *Angew. Chem.* **2017**, *129*, 702 – 729.
[7] a) A. K. Manohar, K. M. Kim, E. Plichta, M. Hendrickson, S. Rawlings, S. R. Narayanan, *J. Electrochem. Soc.* **2016**, *163*, A5118 – A5125; b) K. Gong, F. Xu, J. B. Grunewald, X. Ma, Y. Zhao, S. Gu, Y. Yan, *ACS Energy Lett.* **2016**, *1*, 89 – 93.
[8] L. W. Hruska, R. F. Savinell, *J. Electrochem. Soc.* **1981**, *128*, 18 – 25.
[9] a) S.-E. Chun, B. Evanko, X. Wang, D. Vonlanthen, X. Ji, G. D. Stucky, S. W. Boettcher, *Nat. Commun.* **2015**, *6*, 7818; b) K. Lin, Q. Chen, M. R. Gerhardt, L. Tong, S. B. Kim, L. Eisenach, A. W. Valle, D. Hardee, R. G. Gordon, M. J. Aziz, M. P. Marshak, *Science* **2015**, *349*, 1529 – 1532; c) A. Orita, M. G. Verde, M. Sakai, Y. S. Meng, *Nat. Commun.* **2016**, *7*, 13230.
[10] a) S. J. Dorazio, P. B. Tsitovich, S. A. Gardina, J. R. Morrow, *J. Inorg. Biochem.* **2012**, *117*, 212 – 219; b) V. Maheshwari, J. L. J. Dearling, S. T. Treves, A. B. Packard, *Inorg. Chim. Acta* **2012**, *393*, 318 – 323.
[11] a) G. de Martino Norante, M. Di Vaira, F. Mani, S. Mazzi, P. Stoppioni, *J. Chem. Soc. Dalton Trans.* **1992**, 361 – 365; b) M. Di Vaira, F. Mani, P. Stoppioni, *J. Chem. Soc. Dalton Trans.* **1994**, 3739 – 3743.
[12] D. F. Evans, *J. Chem. Soc.* **1959**, 2003 – 2005.
[13] D. Motoyama, K. Yoshikawa, H. Ozawa, M. Tadokoro, M.-a. Haga, *Inorg. Chem.* **2017**, *56*, 6419 – 6428.
[14] F. Lambert, C. Policar, S. Durot, M. Cesario, L. Yuwei, H. Korri-Youssoufi, B. Keita, L. Nadjo, *Inorg. Chem.* **2004**, *43*, 4178 – 4188.
[15] K. J. Takeuchi, M. S. Thompson, D. W. Pipes, T. J. Meyer, *Inorg. Chem.* **1984**, *23*, 1845 – 1851.
[16] a) A. M. Kosswattaarachchi, A. E. Friedman, T. R. Cook, *ChemSusChem* **2016**, *9*, 3317 – 3323; b) H. Huang, R. Howland, E. Agar, M. Nourani, J. A. Golen, P. J. Cappillino, *J. Mater. Chem. A* **2017**, *5*, 11586 – 11591.
[17] A. Z. Weber, M. M. Mench, J. P. Meyers, P. N. Ross, J. T. Gostick, Q. Liu, *J. Appl. Electrochem.* **2011**, *41*, 1137.
[18] a) B. Hu, C. DeBruler, Z. Rhodes, T. L. Liu, *J. Am. Chem. Soc.* **2017**, *139*, 1207 – 1214; b) E. S. Beh, D. De Porcellinis, R. L. Gracia, K. T. Xia, R. G. Gordon, M. J. Aziz, *ACS Energy Lett.* **2017**, *2*, 639 – 644; c) T. Janoschka, N. Martin, U. Martin, C. Friebe, S. Morgenstern, H. Hiller, M. D. Hager, U. S. Schubert, *Nature* **2015**, *527*, 78 – 81.
[19] K. Wedege, E. Dražević, D. Konya, A. Bentien, *Sci. Rep.* **2016**, *6*, 39101.
[20] R. F. Savinell, J. S. Wainright, U. S. Pat. Appl.: 20, 140,227,574, **2017**.
[21] CCDC 1560025 contains the supplementary crystallographic data for this paper. These data are provided free of charge by The Cambridge Crystallographic Data Centre.

Manuscript received: September 18, 2017
Accepted manuscript online: September 19, 2017
Version of record online: October 18, 2017